

Polarization switching in sliding ferroelectrics: the roles of fluctuation and domain wall

Ziwen Wang and Shuai Dong*

Key Laboratory of Quantum Materials and Devices of Ministry of Education,
School of Physics, Southeast University, Nanjing 211189, China

(Dated: June 9, 2025)

Sliding ferroelectricity is highly attractive for its low energy barriers and fatigue resistance. As the origin of these exotic properties, its unconventional switching dynamics remains poorly understood: how an electric field drives a perpendicular sliding? Taking *h*-BN bilayer as a model system, its switching dynamics is studied using *ab initio* calculations. The off-diagonal Born effective charge leads to the perpendicular relationship between the electric field and ionic movements. Interestingly, the rules of intrinsic coercive field are distinct between *h*-BN bilayer and conventional ferroelectrics. For *h*-BN bilayer, any perturbation breaking the in-plane symmetry plays a key role to assist the avalanche-like switching dynamics. Moreover, the exotic large off-diagonal Born effective charge near the $P = 0$ intermediate state results in a wriggling motion of domain walls in *h*-BN bilayer. Our results reveal the key factors in the ferroelectric switching of sliding ferroelectrics at room temperature.

Introduction. Ferroelectrics are those materials with spontaneous electric polarizations, which are switchable under external electric field. These switchable polarizations have significant impacts for a wide range of technological applications, including nonvolatile memory, sensors, and photonic devices [1, 2]. In the pursuit of higher integration and device miniaturization, ferroelectrics with reduced scale to nanometer are highly demanded. Comparing with conventional ferroelectric films based on three-dimensional oxides, two-dimensional (2D) ferroelectrics have many inborn superiorities and thus have attracted great research enthusiasms in recent years [3–5]. The confirmed members in this family include few-layer CuInP_2S_6 [6, 7], monolayer SnTe [8], $\alpha\text{-In}_2\text{Se}_3$ nanoflakes [9–11], monolayer Bi [12], and so on.

Among these 2D ferroelectrics, a novel branch termed sliding ferroelectrics has been extensively attentioned, which exhibits an unconventional origin of polarizations [13–16]. Specifically, some stacking modes of van der Waals (vdW) layers break the inversion symmetry and thus generate out-of-plane electric dipoles. Then these dipoles can be modulated and even reversed by changing the stacking modes, typically via the interlayer sliding or twisting. Shortly after the theoretical prediction by Wu *et al.* [13], sliding ferroelectricity has been experimentally confirmed in several systems, including WTe_2 bilayer/few-layer [17, 18], bilayer hexagonal BN (*h*-BN) [14, 15]/ $1\text{T}'\text{-ReS}_2$ [19]/ 3R-MoS_2 [20], vdW heterobilayers such as MoS_2/WS_2 [21], as well as an organic-inorganic hybrid crystal [22]. Additionally, its unique switching behaviors have also been investigated, such as the ultrafast switching induced by light and possible polarization switching pathways with multiple interfaces [23–25].

Despite these advances, a fundamental question remains unresolved: how an out-of-plane electric field induces the in-plane sliding motion of atoms/ions? Such a

perpendicular relationship of electrostatic property seems to mimic the Hall effect of electric current, implying plenty emergent physics hidden behind the phenomena. In fact, there are some paradoxes in sliding ferroelectrics. For instance, despite their tiny energy barriers, how can the sliding ferroelectricity persist to room temperature [14, 15, 20]. Moreover, the recently observed high speed of ferroelectric switching remains incompletely understood [26, 27]. Thus, it is crucially important to understand the switching dynamics in sliding ferroelectrics.

In this Letter, the switching dynamics of sliding ferroelectricity is studied using density functional theory (DFT) calculations and *ab initio* molecular dynamics (AIMD) simulations. Among all confirmed sliding ferroelectrics, *h*-BN owns the simplest chemical formula, as well as the largest polarization in this family [16]. Thus, the *h*-BN bilayer will be studied as the model system to reveal the switching dynamics. Details of numerical methods can be found in Supplemental Material (SM) [28]. Our calculations reveal that nonzero off-diagonal element of Born effective charge emerges during the ferroelectric switching process, despite its zero value in the initial ferroelectric state. The required critical electric field shows a progressive reduction accompanying the sliding, implying an avalanche-like behavior, which is different to conventional ferroelectrics like BaTiO_3 where an intrinsic maximum field appears during the polarization reversal. Furthermore, other effects, e.g. wrinkle, layer gap, and temperature, have been investigated, which can modulate the coercive field differentially. Notably, the large off-diagonal Born effective charge near the $P = 0$ intermediate state leads to a wriggling sliding motion of domain walls in multi-domain *h*-BN bilayer, which may be responsible to the high speed of the polarization switching.

Results & discussion. Several possible high-symmetry stacking modes have been proposed for bilayer *h*-BN [29], as illustrated in Fig. 1(a). Among these, the centrosymmetric AA' mode (point group $3m$) is the most stable

* sdong@seu.edu.cn

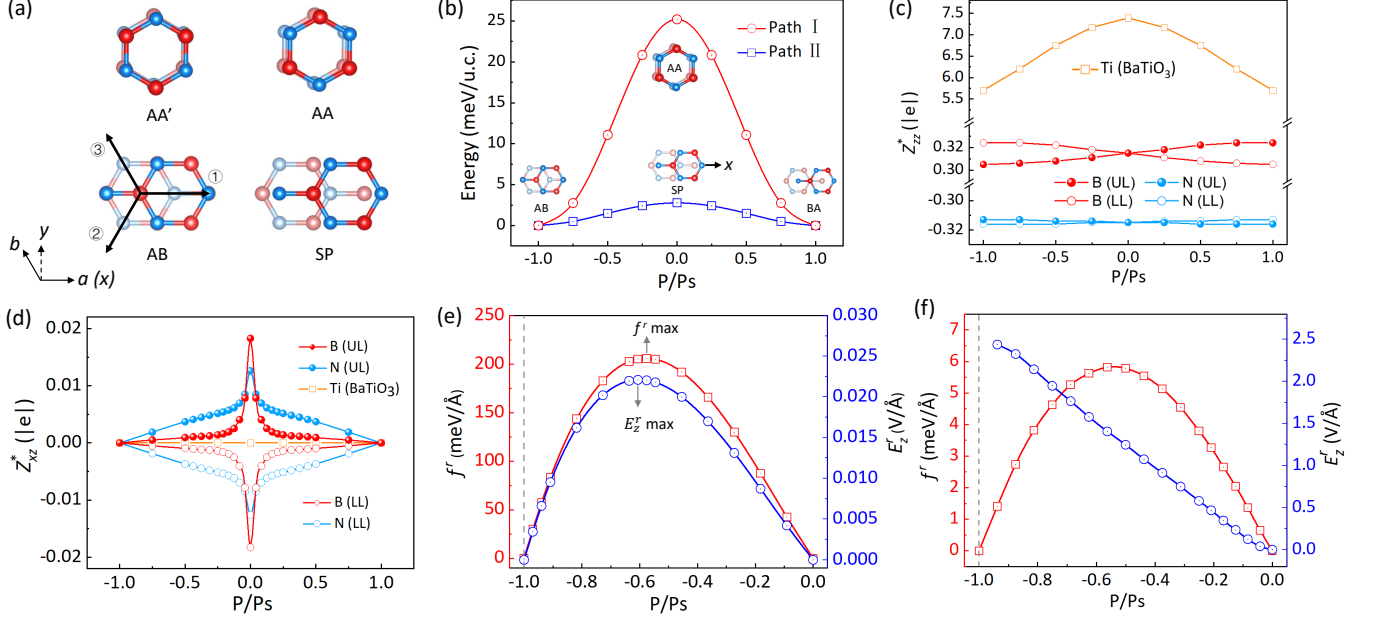


FIG. 1. (a) Top views of AA', AA, AB, and SP (saddle point) stacking modes of *h*-BN bilayer. The in-plane C_3 symmetry is denoted by black arrows in the AB mode. (b) Calculated energy barriers of two switching pathways of *h*-BN bilayer. Inset: Four typical configurations during the switching. AB: $+P$, AA or SP: $P = 0$, BA: $-P$. (c-d) Tensor elements of Born effective charge in *h*-BN bilayer, in comparison with BaTiO₃. (e) Diagonal element Z_{zz}^* . (f) Off-diagonal element Z_{xz}^* . UL: Upper layer. LL: Lower layer. (e-f) The intrinsic resistance force f^r and required critical electric field E_z^* during the polarization switching: (e) BaTiO₃. (f) *h*-BN bilayer.

one, while the AB (or BA) mode (polar point group $3m$) is the first metastable one. Both AA' and AB have been experimentally observed in bilayer *h*-BN [14, 30]. Noting that the AA' and AB modes can not be interconverted via the interlayer sliding operation, but can be interconverted via the 60° interlayer twisting operation plus the sliding operation.

A spontaneous polarization is expected in the AB (BA) stacking mode, which originates from the asymmetric vertical alignment of N and B atoms of different layers. The distortion of the p_z orbital of N ion results in a net out-of-plane electric dipole [15]. The degenerate AB and BA stacking can be interconverted through interlayer sliding of BN layers, leading to the reversal of ferroelectric polarization. Two distinct ferroelectric switching pathways have been examined: AB \rightarrow AA \rightarrow BA (Path I) and AB \rightarrow SP \rightarrow BA (Path II). The energy barrier for Path II is much lower than that of Path I [Fig. 1(b)], consistent with previous studies [23, 24]. Therefore, only the Path II will be considered in the following.

As stated before, it is not so intuitive how an electric field drives collective motion of ions perpendicularly. This paradox can be understood within the framework of Born effective charge [31, 32]. The Born effective charge Z^* is a tensor:

$$Z_{\kappa,ij}^* = \Omega \frac{\partial P_j}{\partial u_{\kappa,i}} = -\frac{\partial^2 F}{\partial E_j \partial u_{\kappa,i}} = \frac{\partial f_{\kappa,i}^E}{\partial E_j}, \quad (1)$$

where κ is the index of ions; i and $j \in \{x, y, z\}$ are three

orthogonal orientations. P , u , F , E , and Ω denote the polarization, ion position, electric enthalpy, external electric field, and unit-cell volume, respectively. To drive the ion motion, the electrostatic force f^E on the κ -ion under electric field E can be expressed as:

$$f_{\kappa,i}^E = \sum_j E_j Z_{\kappa,ij}^*. \quad (2)$$

During the switching, the external electric field should be large enough to overcome the intrinsic resistance from energy barrier, which can be expressed as $f_{\kappa,i}^r = -\partial H / \partial u_{\kappa,i}$ where H is the Hamiltonian. The coercive field E^c is defined as the maximum value of the required critical electric field E^r during the polarization reversal.

Taking the conventional ferroelectric as an example, e.g. tetragonal perovskite BaTiO₃, its Born effective charge tensor Z^* is diagonal, while all off-diagonal elements are zero [33]. During the ferroelectric switching between $\pm P$ (along the z -axis), the related Z_{zz}^* obtained in our density functional perturbation theory (DFPT) calculation of the core ion Ti is shown in Fig. 1(c), which is rather large and evolves moderately as a function of P . The complete Born effective charge tensor for barium and oxygen ions are provided in Fig. S1 of SM [28]. Then the intrinsic resistance force f^r (on positive ions) during the switching is estimated in Fig. 1(e), which starts from zero and reaches its maximum in the middle, corresponding to the steepest slope of the energy barrier (Fig. S2 of SM [28]). The required critical electric field E_z^* to over-

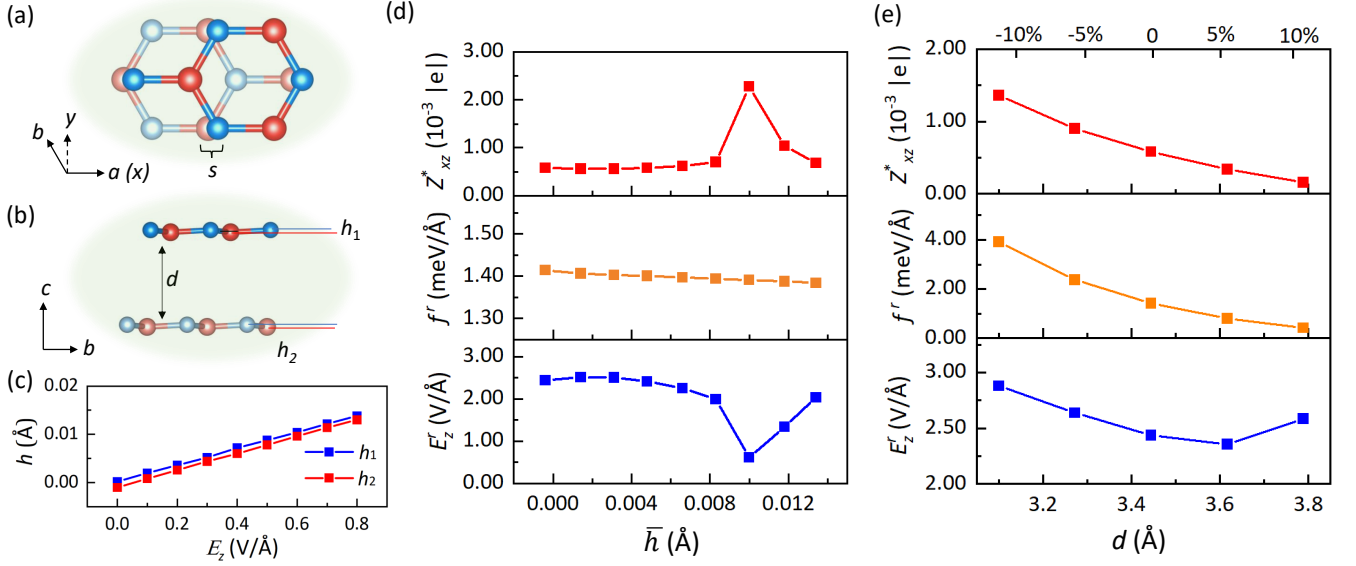


FIG. 2. (a) Top view of the tiny sliding s along the x -direction from the original AB stacking one. (b) Side view of the wrinkled structure. h_1 and h_2 : the wrinkled heights of the upper and lower layer, respectively. d : the layer gap. (c) The evolution of wrinkled amplitudes as a function of vertical electric field E_z . (d-e) Effects of the layer wrinkle \bar{h} and layer gap d . Upper: the sum of off-diagonal Z_{xz}^* of B and N ions of the upper layer. The Z_{xz}^* of lower layer is exactly opposite (not shown here). Middle: the intrinsic resistance force f^r of one layer. Lower: the estimated required critical electric field E_z^r . (d) \bar{h} -dependent properties at the optimal $d = 3.44$ Å. (e) d -dependent properties without wrinkle.

come such resistance force is derived from Eq. 2, as shown in Fig. 1(e), which shows a similar tendency to f^r . The moderate P -dependence of Z_{zz}^* leads to slight difference between the peaks of f^r and E_z^r . In short, the E_z^r for BaTiO₃'s (single-domain) switching is a climbing-like behavior with the maximum appearing around the peak of resistance force.

In contrast, the Z_{zz}^* of B and N ions in h -BN bilayer are much smaller, implying weaker ionic behavior. More importantly, nonzero off-diagonal Z_{xz}^* appears (except for the initial and end states), as shown in Fig. 1(d), which is responsible for the perpendicular relationship between electric field and sliding motion. The Z_{xz}^* 's of N and B ions of one layer own the same sign, implying the same-direction motion under a perpendicular electric field, i.e. the horizontal sliding instead of wrinkling. The values of Z_{xz}^* 's are much smaller than their corresponding Z_{zz}^* 's. An important fact is that Z_{xz}^* 's change drastically during the switching process, leading to a sharp peak at the $P = 0$ state (i.e. the SP mode). The zero-value of Z_{xz}^* 's at the initial and end states (i.e. the AB and BA modes) is due to the in-plane C_3 rotational symmetry of the hexagonal lattice. In other words, there are three equivalent sliding paths with 120° interval for the AB \rightarrow SP \rightarrow BA switching. Then an out-of-plane electric field can not break the C_3 rotational symmetry, and thus can not determine which one of the three is preferred. Thus the Z_{xz}^* at the AB and BA modes should be exact zero.

These characteristics of Z_{xz}^* 's lead to a nontrivial switching process for h -BN bilayer, as shown in Fig. 1(f). Although the tendency of force f^r looks similar to that

of BaTiO₃ which starts from zero and reaches the maximum in the middle, the required critical electric field E_z^r exhibits totally different behaviors. At the initial ferroelectric state (e.g. the AB mode), the zero Z_{xz}^* 's make the system stable against the out-of-plane electric field. Only after a finite sliding, E_z^r becomes finite and monotonously decreases with sliding (e.g. decreasing P). Thus, the largest E_z^r is not an intrinsic constant, but determined by the initial sliding conditions, which can be affected by many extrinsic factors that break the initial C_3 symmetry, such as thermal fluctuations, twist angles, as well as domain walls (to be discussed later). In short, the behavior of E_z^r for sliding switching is avalanche-like, in contrast to conventional climbing-like behavior. This mechanism also applies to other sliding ferroelectrics with C_3 rotational symmetry, such as 3R-MoS₂ bilayer and WS₂/MoS₂ heterobilayer, as shown in Figs.S3-S6 of SM [28].

Beginning from a staggered stacking mode with tiny sliding $s = 0.045$ Å [Fig. 2(a)], the calculated vertical coercive field E_z^c is 2.43 V/Å. Such a coercive field E_z^c is higher than the experimental measured values (~ 0.03 V/Å) for nearly two orders of magnitude [14]. Thus, other factors should be considered to give a more realistic description.

Intuitively, the vertical wrinkling of h -BN will be induced by the out-of-plane electric field. The heterocharge Z_{zz}^* 's of B and N ions [Fig. 1(c)] lead to opposite displacements along the z -axis under the vertical electric field E_z . The structure is optimized under the vertical electric field, and the layer thickness h is defined to quan-

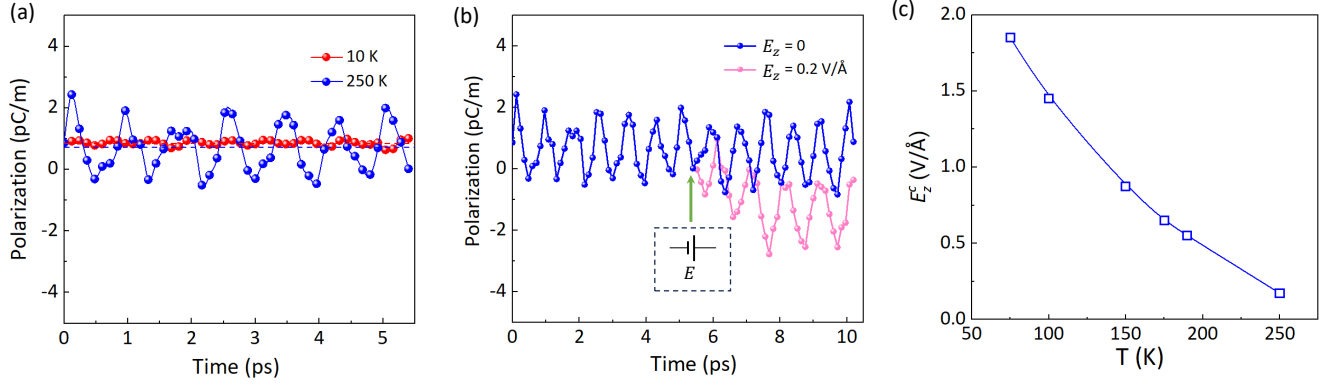


FIG. 3. AIMD simulations of *h*-BN bilayer. (a) Time dependent polarization under different temperatures without the electric field. The average values of polarization are depicted in dotted lines. (b) Time dependent polarization under 250 K with/without the electric field ($E_z = 0.2$ V/Å). The electric field is turn on at 5.4 ps. (c) Temperature dependence of the magnitude of coercive field E_z^c estimated from AIMD simulation.

titatively characterize this wrinkling effect [Fig. 2(b)]. As shown in Fig. 2(c), h grows linearly with increasing E_z , and the wrinkling is almost identical between two layers (h_1 is only slightly larger than h_2 due to the existence of polarization). However, the in-plane C_3 symmetry remains preserved, despite the wrinkling. Therefore, the avalanche-like behavior of E_z^r will not be qualitatively altered by the wrinkling. Then the physical properties with wrinkling are recalculated by starting from a slightly staggered configuration $s = 0.045$ Å, as summarized in Fig. 2(d). With increasing wrinkling amplitude [characterized using $\bar{h} = (h_1 + h_2)/2$], the Z_{xz}^* is almost a constant in the beginning, but owns a peak at $\bar{h} = 0.01$ Å. Meanwhile, the intrinsic resistance force f^r on each layer is almost a constant. Consequently, E_z^r will be significantly reduced at the peak of Z_{xz}^* . For example, $E_z^r \sim 0.61$ V/Å for $s = 0.045$ Å at $\bar{h} = 0.01$ Å, only $\sim 1/4$ of the original one without wrinkling. In short, the vertical wrinkling, induced by the perpendicular electric field, can significantly lower E_z^r only at a specific amplitude of vertical wrinkling.

Besides the vertical wrinkling, another tunable structural degree of freedom is the interlayer gap d , which is directly related to the sliding ferroelectricity [34, 35]. Also taking the staggered $s = 0.045$ Å (and without the vertical wrinkling), the off-diagonal Z_{xz}^* and f^r are recalculated as a function of interlayer gap d . As shown in Fig. 2(e), both Z_{xz}^* and f^r change monotonously: the larger d , the smaller Z_{xz}^* and f^r . Then the E_z^r , as a result of f^r/Z_{xz}^* , is not monotonous, which reaches a minimum at $d = 3.62$ Å (slightly larger than the original d). The minimum $E_z^r \sim 1.90$ V/Å is only 22% lower than the original one.

Above study has demonstrated that an initial nonzero s is mandatory for sliding dynamics, while the vertical wrinkling and interlayer gap can affect this process. In real situations at finite temperatures, the comprehensive effect can be simulated using AIMD. As shown in Fig. 3(a), at 10 K without external fields, the AB stack-

ing mode is stable, with a ferroelectric $P_z \sim 0.82$ pC/m. By increasing temperature to 250 K, the thermal fluctuation is enhanced while an average $P_z \sim 0.78$ pC/m is maintained. When an out-of-plane electric field $E_z = 0.2$ V/Å is applied at 250 K, the polarization can be easily switched within a short time, as shown in Fig. 3(b). The required amplitudes of the coercive field E_z^c at different temperatures obtained in AIMD are summarized in Fig. 3(c), which steeply decreases with increasing temperature. It is reasonable since the strong thermal fluctuations at high temperatures can trigger the avalanche-like switching more easily. Thus, the experimental coercive field at room temperature should be greatly suppressed, due to large s from strong thermal fluctuations instead of the intuitional scenario of low energy barrier.

Finally, it is worth to investigate the effect of domain wall on the sliding dynamics. Previous experiments have observed the high speed of domain wall motion in the polarization switching process.[20, 26]. Given the largest off-diagonal Z_{xz}^* in the symmetric intermediate SP state, the center region of domain wall is naturally expected to exhibit a much larger Z_{xz}^* than that within flanks. Then the center region will be more sensitive to external field and thus plays as the pioneer of sliding dynamics.

To simulate the domain wall, a supercell containing $+P$, $-P$, and domain wall is constructed, as shown in Fig. 4(a). By fixing the $+P$ and $-P$ domains and relaxing domain walls, the profile of local P , characterized by the sliding distance x , is shown in Fig. 4(b). The sliding distance x changes continuously from $+P$ to $-P$ states. Then elements of the off-diagonal Born effective charge Z^* for each unit cell are calculated. As shown in Fig. 4(c), the center regions of domain walls own relative larger Z_{xz}^* values, and even within the domains Z_{xz}^* 's become non-zero due to the proximity effect of domain walls. Furthermore, the off-diagonal Z_{yz}^* element is also induced which further enhances the sliding. Thus, the center region of domain wall will achieve a much larger accelerated velocity and move faster than the flank regions when a verti-

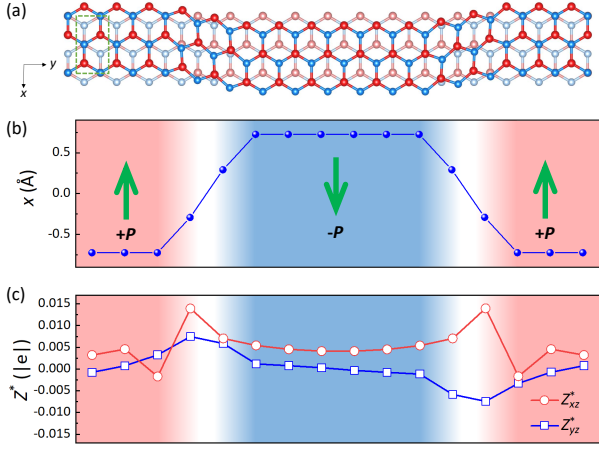


FIG. 4. (a) Sketch of domain walls between two ferroelectric domains. Here the orthorhombic cell is taken as the unit cell, as depicted by the green rectangle. (b) The sliding distance of each unit cell (x) over the ferroelectric domains and domain walls. The domain regions with positive and negative polarization are denoted in green arrows and different background colors. The gradient background color regions denote the domain walls. (c) The off-diagonal Born effective charge elements Z^*_{xz} and Z^*_{yz} of each unit cell in the upper layer. The Z^*_{xz} and Z^*_{yz} become larger at center regions of domain walls.

cal electric field is applied. This out-of-sync acceleration will generate wriggling and the faster-moving center region will pull the non-center regions, further accelerate the domain wall motion. In the subsequent moment, the

newly formed center region induces the wriggling motion continuously and increases the domain wall velocity again until the complete ferroelectric switching process is finished. This characteristic may be responsible for the high speed of the ferroelectric switching observed in experiments, warranting further investigation.

In summary, the switching dynamics of sliding ferroelectric h -BN bilayer has been investigated numerically, which is nontrivially different from conventional ferroelectrics. It is the nonzero off-diagonal element of Born effective charge leading to perpendicular relationship between electric field and sliding motion. To start the sliding, perturbation induced by extrinsic factors such as thermal fluctuation, is needed to break the C_3 symmetry of the initial ferroelectric state. The required critical electric field E_z^r of a single domain does not have an intrinsic maximum, conceptually different from conventional ferroelectrics like BaTiO_3 . Layer wrinkle, layer gap, temperature, as well as domain wall can be helpful to reduce the ferroelectric coercive field.

Note: We became aware of two recent preprints on the switching dynamics of sliding ferroelectrics [36, 37]. In ref. [36], their work also highlighted the key effects of off-diagonal Born effective charges and domain walls. In ref. [37], an undamped soliton-like domain wall motion was reported [37].

ACKNOWLEDGMENTS

We thank Dr. Peng Chen and Dr. Junjie Zhang for helpful discussions. Work was supported by National Natural Science Foundation of China (Grant Nos. 12325401, 12274069, and 123B2053) and the Big Data Computing Center of Southeast University.

-
- [1] J. F. Scott, Applications of modern ferroelectrics, *Science* **315**, 954 (2007).
 - [2] K. Rabe, C. H. Ahn, and J.-M. Triscone, eds., *Physics of Ferroelectrics: A Modern Perspective* (Springer, 2007).
 - [3] S. Li, F. Wang, Y. Wang, J. Yang, X. Wang, X. Zhan, J. He, and Z. Wang, Van der waals ferroelectrics: Theories, materials, and device applications, *Adv. Mater.* **36**, 2301472 (2024).
 - [4] C. Wang, L. You, D. Cobden, and J. Wang, Towards two-dimensional van der waals ferroelectrics, *Nat. Mater.* **22**, 542 (2023).
 - [5] Z. Guan, H. Hu, X. Shen, P. Xiang, N. Zhong, J. Chu, and C. Duan, Recent progress in two-dimensional ferroelectric materials, *Adv. Electron. Mater.* **6**, 1900818 (2020).
 - [6] A. Belianinov, Q. He, A. Dziazgys, P. Maksymovych, E. Eliseev, A. Borisevich, A. Morozovska, J. Banys, Y. Vysochanskii, and S. V. Kalinin, CuInP_2S_6 room temperature layered ferroelectric, *Nano Lett.* **15**, 3808 (2015).
 - [7] F. Liu, L. You, K. L. Seyler, X. Li, P. Yu, J. Lin, X. Wang, J. Zhou, H. Wang, H. He, *et al.*, Room-temperature ferroelectricity in CuInP_2S_6 ultrathin flakes, *Nat. Commun.* **7**, 12357 (2016).
 - [8] K. Chang, J. Liu, H. Lin, N. Wang, K. Zhao, A. Zhang, F. Jin, Y. Zhong, X. Hu, W. Duan, *et al.*, Discovery of robust in-plane ferroelectricity in atomic-thick snte, *Science* **353**, 274 (2016).
 - [9] C. Cui, W.-J. Hu, X. Yan, C. Addiego, W. Gao, Y. Wang, Z. Wang, L. Li, Y. Cheng, P. Li, X. Zhang, H. N. Alsharreef, T. Wu, W. Zhu, X. Pan, and L.-J. Li, Intercorrelated in-plane and out-of-plane ferroelectricity in ultrathin two-dimensional layered semiconductor In_2Se_3 , *Nano Lett.* **18**, 1253 (2018).
 - [10] J. Xiao, H. Zhu, Y. Wang, W. Feng, Y. Hu, A. Dasgupta, Y. Han, Y. Wang, D. A. Muller, L. W. Martin, P. Hu, and X. Zhang, Intrinsic two-dimensional ferroelectricity with dipole locking, *Phys. Rev. Lett.* **120**, 227601 (2018).
 - [11] Y. Zhou, D. Wu, Y. Zhu, Y. Cho, Q. He, X. Yang, K. Herrera, Z. Chu, Y. Han, M. C. Downer, H. Peng, and K. Lai, Out-of-plane piezoelectricity and ferroelectricity in layered α - In_2Se_3 nanoflakes, *Nano Lett.* **17**, 5508 (2017).
 - [12] J. Gou, H. Bai, X. Zhang, Y. L. Huang, S. Duan, A. Ariando, S. A. Yang, L. Chen, Y. Lu, and A. T. S. Wee, Two-dimensional ferroelectricity in a single-element bismuth monolayer, *Nature* **617**, 67 (2023).

- [13] L. Li and M. Wu, Binary compound bilayer and multilayer with vertical polarizations: Two-dimensional ferroelectrics, multiferroics, and nanogenerators, *ACS Nano* **11**, 6382 (2017).
- [14] M. V. Stern, Y. Waschitz, W. Cao, I. Nevo, K. Watanabe, T. Taniguchi, E. Sela, M. Urbakh, O. Hod, and M. B. Shalom, Interfacial ferroelectricity by van der waals sliding, *Science* **372**, 1462 (2021).
- [15] K. Yasuda, X. Wang, K. Watanabe, T. Taniguchi, and P. Jarillo-Herrero, Stacking-engineered ferroelectricity in bilayer boron nitride, *Science* **372**, 1458 (2021).
- [16] M. Wu and J. Li, Sliding ferroelectricity in 2D van der Waals materials: Related physics and future opportunities, *Proc. Natl. Acad. Sci. U. S. A.* **118**, e2115703118 (2021).
- [17] Z. Fei, W. Zhao, T. A. Palomaki, B. Sun, M. K. Miller, Z. Zhao, J. Yan, X. Xu, and D. H. Cobden, Ferroelectric switching of a two-dimensional metal, *Nature* **560**, 336 (2018).
- [18] J. Xiao, Y. Wang, H. Wang, C. Pemmaraju, S. Wang, P. Muscher, E. J. Sie, C. M. Nyby, T. P. Devereaux, X. Qian, X. Zhang, and A. M. Lindenberg, Berry curvature memory through electrically driven stacking transitions, *Nat. Phys.* **16**, 1028 (2020).
- [19] Y. Wan, T. Hu, X. Mao, J. Fu, K. Yuan, Y. Song, X. Gan, X. Xu, M. Xue, X. Cheng, C. Huang, J. Yang, L. Dai, H. Zeng, and E. Kan, Room-Temperature Ferroelectricity in 1T'-ReS₂ Multilayers, *Phys. Rev. Lett.* **128**, 067601 (2022).
- [20] R. Bian, R. He, E. Pan, Z. Li, G. Cao, P. Meng, J. Chen, Q. Liu, Z. Zhong, W. Li, and F. Liu, Developing fatigue-resistant ferroelectrics using interlayer sliding switching, *Science* **385**, 57 (2024).
- [21] L. Rogée, L. Wang, Y. Zhang, S. Cai, P. Wang, M. Chhowalla, W. Ji, and S. P. Lau, Ferroelectricity in untwisted heterobilayers of transition metal dichalcogenides, *Science* **376**, 973 (2022).
- [22] L.-P. Miao, N. Ding, N. Wang, C. Shi, H.-Y. Ye, L. Li, Y.-F. Yao, S. Dong, and Y. Zhang, Direct observation of geometric and sliding ferroelectricity in an amphidynamic crystal, *Nat. Mater.* **21**, 1158 (2022).
- [23] Q. Yang and S. Meng, Light-induced complete reversal of ferroelectric polarization in sliding ferroelectrics, *Phys. Rev. Lett.* **133**, 136902 (2024).
- [24] J. Wang, X. Li, X. Ma, L. Chen, J.-M. Liu, C.-G. Duan, J. Íñiguez González, D. Wu, and Y. Yang, Ultrafast switching of sliding polarization and dynamical magnetic field in van der Waals bilayers induced by light, *Phys. Rev. Lett.* **133**, 126801 (2024).
- [25] J. Liang, D. Yang, J. Wu, Y. Xiao, K. Watanabe, T. Taniguchi, J.I. Dadap, and Z. Ye, Resolving polarization switching pathways of sliding ferroelectricity in trilayer 3R-MoS₂, *Nat. Nanotechnol.* (2025).
- [26] K. Yasuda, E. Zalys-Geller, X. Wang, D. Bennett, S. S. Cheema, K. Watanabe, T. Taniguchi, E. Kaxiras, P. Jarillo-Herrero, and R. Ashoori, Ultrafast high-endurance memory based on sliding ferroelectrics, *Science* **385**, 53 (2024).
- [27] R. He, B. Zhang, H. Wang, L. Li, P. Tang, G. Bauer, and Z. Zhong, Ultrafast switching dynamics of the ferroelectric order in stacking-engineered ferroelectrics, *Acta Mater.* **262**, 119416 (2024).
- [28] See Supplemental Material [url] for methods, complete Born effective charge tensor of barium and oxygen of BaTiO₃; energy barrier of the switching path of BaTiO₃; lattice constant and polarization of h-BN bilayer with different exchange-correlation functionals and vdW corrections; structures, energy barriers of the switching path, off-diagonal Born effective charges, intrinsic resistance force and required critical electric field during the polarization switching of 3R-MoS₂ bilayer and WS₂/MoS₂ heterobilayer; including Refs. [13, 24? ? ? ? ? ? ? ? ?].
- [29] G. Constantinescu, A. Kuc, and T. Heine, Stacking in bulk and bilayer hexagonal boron nitride, *Phys. Rev. Lett.* **111**, 036104 (2013).
- [30] J. H. Warner, M. H. Rümmeli, A. Bachmatiuk, and B. Büchner, Atomic resolution imaging and topography of boron nitride sheets produced by chemical exfoliation, *ACS Nano* **4**, 1299 (2010).
- [31] X. Gonze and C. Lee, Dynamical matrices, born effective charges, dielectric permittivity tensors, and interatomic force constants from density-functional perturbation theory, *Phys. Rev. B* **55**, 10355 (1997).
- [32] P. Ghosez and X. Gonze, Band-by-band decompositions of the born effective charges, *J. Phys.: Condens. Matter* **12**, 9179 (2000).
- [33] P. Ghosez, J.-P. Michenaud, and X. Gonze, Dynamical atomic charges: the case of ABO₃ compounds, *Phys. Rev. B* **58**, 6224 (1998).
- [34] Z. Wang and S. Dong, Large in-plane negative piezoelectricity and giant nonlinear optical susceptibility in elementary ferroelectric monolayers, *Phys. Rev. B* **108**, 235423 (2023).
- [35] N. Ding, J. Chen, C. Gui, H. You, X. Yao, and S. Dong, Phase competition and negative piezoelectricity in interlayer-sliding ferroelectric ZrI₂, *Phys. Rev. Mater.* **5**, 084405 (2021).
- [36] C. Ke, F. Liu, and S. Liu, Superlubric motion of wave-like domain walls in sliding ferroelectrics (2025), arXiv:2502.01007.
- [37] Y. Shi, Y. Gao, R. He, H. Wang, B. Zhang, and Z. Zhong, Undamped soliton-like domain wall motion in sliding ferroelectrics (2025), arXiv:2502.02137.